Materials Letters 269 (2020) 127675

Contents lists available at ScienceDirect

Materials Letters

journal homepage: www.elsevier.com/locate/mlblue

Impact of CsI concentration, relative humidity, and annealing temperature on lead-free Cs_2SnI_6 perovskites: Toward visible light photodetectors application

Mokurala Krishnaiah [1], Md. Mohibul Islam Khan [1], Ajit Kumar, Sung Hun Jin *

Department of Electronic Engineering, Incheon National University, Incheon 406-772, Republic of Korea

ARTICLE INFO

Article history:
Received 9 February 2020
Received in revised form 11 March 2020
Accepted 17 March 2020
Available online 19 March 2020

Keywords:
CsI concentration
Annealing temperature
RH% levels
Structural
Electrical and photodetection properties

ABSTRACT

Physical, electrical, and photodetection properties of stable, lead-free Cs_2SnI_6 (CSI) perovskite thin films prepared on thermally oxidized Si (SiO_2, 100 nm) substrates via direct solution spin coating process are reported. XRD, XPS, and EDS analysis reveal that initial CsI rich-concentration, higher RH% levels (>40%) have an impact on phase formation of CSI films. The porous, sub-μm sized rods of fabricated CSI films are confirmed by FEG-SEM analysis. Contact resistance (R_c) and sheet resistance (R_{sh}) for CSI films, annealed at 150 °C, are decreased up to 37% and 85%, respectively, as compared with those of films processed at 75 °C. The photoresponsivity (6 mA/W) and specific detectivity (2.00×10^9 Jones) for two-terminal CSI photodetectors are achieved with annealing condition of 100℃ and at a bias voltage of 1 V as well. The preliminary photodetection properties for CSI devices processed at low temperatures indicate that they can be potentially applicable to a flexible, visible light photodetector.

1. Introduction

Earth-abundant, lead-free, relatively air stable Cs_2SnI_6 (CSI) double perovskite has striking properties such as ambipolar nature, excellent mobility (1–509 $cm^2 V^{-1} s^{-1}$), high absorption coefficient (10^5 cm^{-1}) in the visible region, direct-bandgap (1.3 eV) [1–6]. Due to these attractive features, it has explored many potential optoelectronic device applications such as field-effect transistors [3], photodetectors [4], photoelectrochemical water splitting [7], light absorbers, and hole transport layers for solar cells [1–2,5,8]. Synthesis of single-phase CSI films has a challenge due to the narrow chemical potential window [6]. As per previous studies [4,5], the Sn-rich precursor concentration is favorable for the formation of pure phase CSI nanostructures [4,5]. Reported CSI films in literature were fabricated on soda-lime glasses (SLG), fluorine-doped tin oxide (FTO), and indium tin oxide (ITO) substrates [1–2,4–10] via as a direct solution coating process (e.g., spin coating, and aerosol-assisted chemical vapor deposition) [2,6], co-evaporation [6,9], hybrid process (i.e., thermal evaporation of CsI films, followed by SnI_4 vapor treatment or spin/spray coating technique of SnI_4 solution) [8–10]. It has been reported that the formation of single-phase CSI films is critically affected by annealing temperature/time, atmosphere, and fabrication methods [6–10]. However, the effect of the Cs/Sn ratios on the phase formation of CSI films on Si substrates via direct solution spin coating is yet to be addressed. The effect of thermal stability, moisture, and humidity level on prepared films (synthesized and phase formed Cs_2SnI_6 particles) were reported [11–13]. Furthermore, the influence of relative humidity levels (RH%) on phase formation of CSI films during the direct solution spin coating process has not been reported in the literature. Thus, it is highly essential to study process parameters on the phase formation of CSI films in ambient conditions.

In this work, we report on the fabrication of Cs_2SnI_6 (CSI) films on Si substrates via direct solution spin coating process. The effect of initial CsI concentrations, annealing temperatures on chemical composition, morphology, and phase formation of CSI films is investigated. Preliminary results of photodetection on CSI PDs, prepared at low temperature, suggest that these can be applicable to flexible, visible photodetectors.

2. Experimental details and characterization tools

The effect of initial CsI concentration, annealing temperature, and RH% levels on Cs_2SnI_6 (CSI) phase formation is investigated in the present study. In brief, two different CSI solutions made from two CsI concentrations (1.60 mmol and 2 mmol) with constant

* Corresponding author.
E-mail address: shjin@inu.ac.kr (S.H. Jin).
[1] These authors are equally contributed to this work.

https://doi.org/10.1016/j.matlet.2020.127675
0167-577X/

1 mmol SnI_4 were utilized to examine their effects on morphology, chemical composition, phase formation of CSI films, corresponding to each annealing temperature in a vacuum oven. The solution with a fixed CsI concentration (i.e, 1.60 mmol) was selected and spin-coated on oxidized Si substrates to investigate into effects on phase formation of CSI film, corresponding to RH%, 30%, 40%, 50%, 60%, and 80%, respectively, in the lab. Moreover, annealing temperature effects on electrical properties for CSI films were also studied with a fixed 1.60 mmol CsI concentration. The specific conditions for CSI film formation, device fabrication steps, and characterization tools are addressed in Supporting information.

3. Results and discussion

The effect of initial CsI concentration, annealing temperature, and different RH% levels on CSI phase formation is investigated via XRD analysis (Fig. 1a–c). The XRD patterns for CSI films with 2 mmol CsI show a dominant impurity phase of CsI (JCPDF No.: 060311) along with the cubic CSI phase (JCPDF No.: 51-0466) for all annealing conditions (Fig. 1a). All diffraction peaks in the XRD patterns of CSI films, prepared with 1.6 mmol CsI, match with the CSI phase (Fig. 1b). The pure CSI phase formation is observed only in the films processed in the RH% levels <40% conditions (Fig. 1c). The impurity CsI phase is detected together with the CSI phase for films made in all other higher RH% conditions (Fig. 1c). The maximum intensity along (4 0 0) peak indicates the unidirectional growth of the fabricated CSI films [4]. The surface morphology and the raw data of the average chemical composition of fabricated CSI films are summarized in the Supporting information (Figs. S1–S12, Tables S1–S8). All films processed with 2 mmol CsI resulted in higher Cs-rich, Sn-rich, and higher I–deficiency composition as compared with 1.60 mmol CsI (Figs. 1d and S1). The Cs/Sn ratio varies from 1.87 ± 0.09 to 2.38 ± 0.02 and 1.75 ± 0.05 to 1.80 ± 0.03 for CSI films prepared with 2 mmol CsI and 1.6 mmol CsI while an increase in annealing temperature from 75 °C to 150 °C for 15 min, respectively (Fig. 1d). The Cs-rich chemical composition leads to the formation of the secondary phase (CsI) along with the main CSI phase, which is consistent with the results in the literature [2,8]. The near-stoichiometric Cs, Sn-rich, and I-deficiency might be a possible reason for the formation of pure phase CSI films fabricated with Sn-rich initial precursor concentration (1.6 mmol CsI) [4,5]. The obtained chemical composition is in good agreement with XRD analysis.

The surface morphology of CSI films annealed at different temperatures is studied by FEG-SEM analysis (Fig. 2(a–d)). The dendritic and spherical-like morphology is observed for films annealed at 75 °C (Fig. 2a). The porous, sub-μm-sized rods are noticed in the films at higher annealing temperatures >100 °C (Fig. 2b, c). The diameter of sub-μm rods is estimated to be 600 nm–800 nm. As per previous studies, precursor concentration, and moisture, annealing temperature/time, solvent/solvent evaporation rate affect the morphology of perovskite films [14,15]. Based on the literature, we speculate that the DMF solvent has a unique role in the submicron-rods formation and some of their vertical alignment [14,15]. However, the mechanism on the formation of sub-μm rods is not clear yet. The clarification of the exact role of DMF on the formation of different solvatomorphs will be the subject of further studies. The impurity phase (CsI) and chemical composition of fabricated CSI films, annealed at 100 °C for 15 °C min, were further confirmed by XPS analysis. The scan survey spectra of XPS and core level spectra of the constituent elements of fabricated CSI films are shown in Fig. S13. All constituent elements Cs,

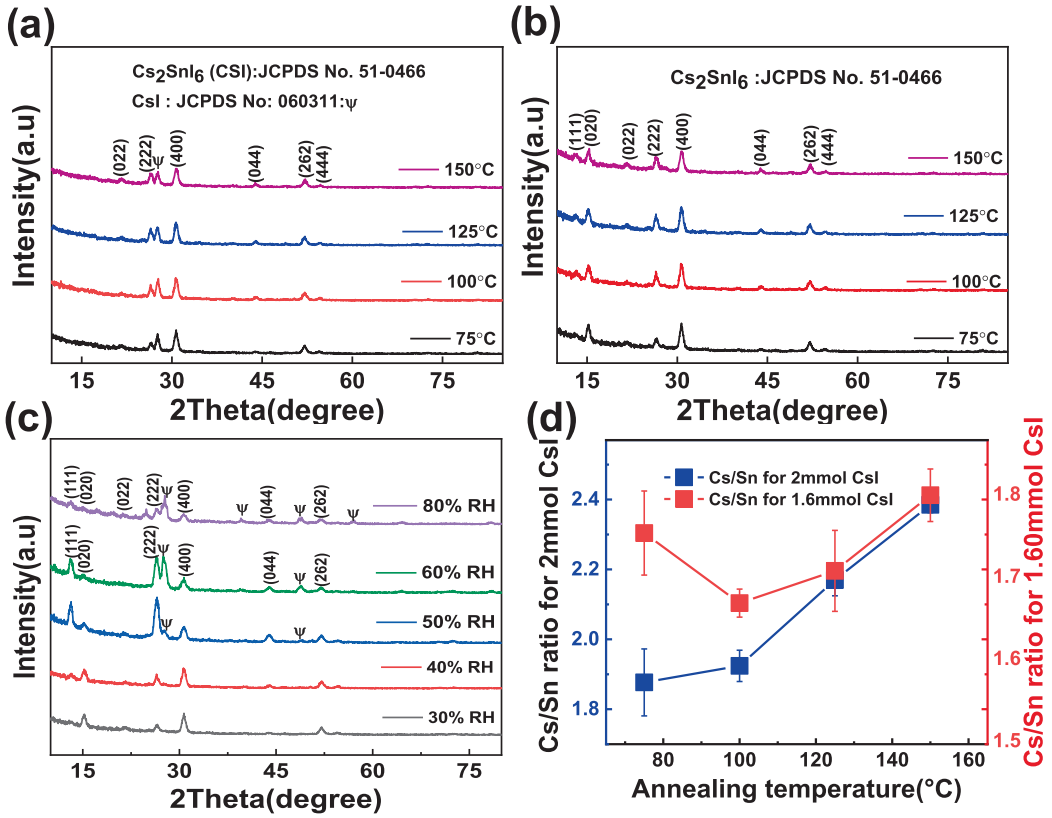

Fig. 1. Phase analysis of CSI films: CSI films fabricated with (a) 2 mmol CsI, (b) 1.6 mmol CsI and annealed at 75 °C to 150 °C for 15 min and (c) CSI films processed in different relative humidity levels and annealed at 100 °C for 15 min in vacuum (d) influence of CsI concentration on Cs/Sn ratio of CSI films processed at different annealing temperatures.

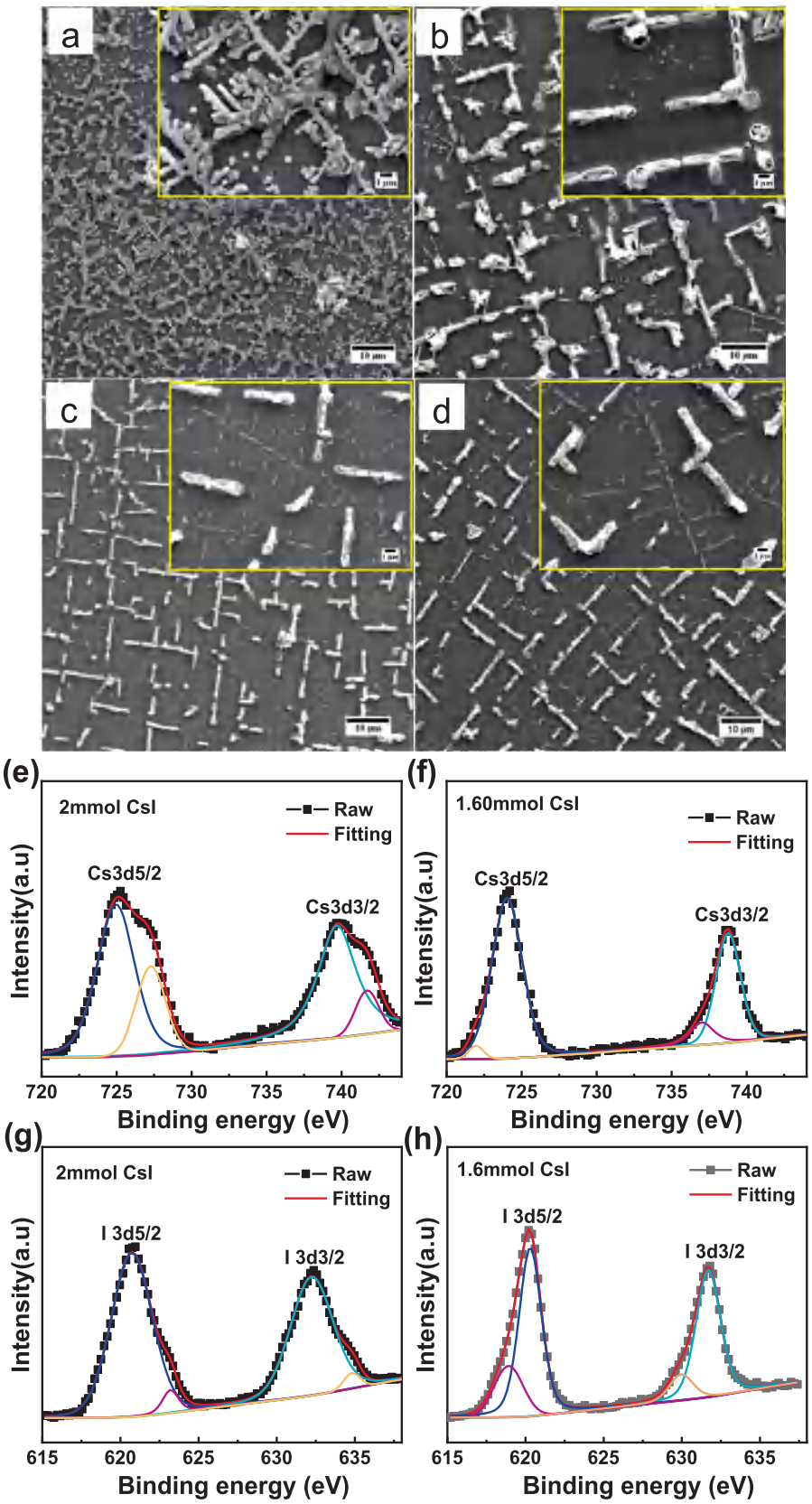

Fig. 2. SEM images for morphology of CSI films annealed at (a) 75 °C, (b) 100 °C, (c) 125 °C, and (d) 150 °C for 30 min and XPS analysis of CSI films fabricated with 1.6 mmol and 2.00 mmol CsI and annealed at 100 °C for 15 min: (e) and (f) core level spectra of Cs, (g) and (h) core level spectrum of I.

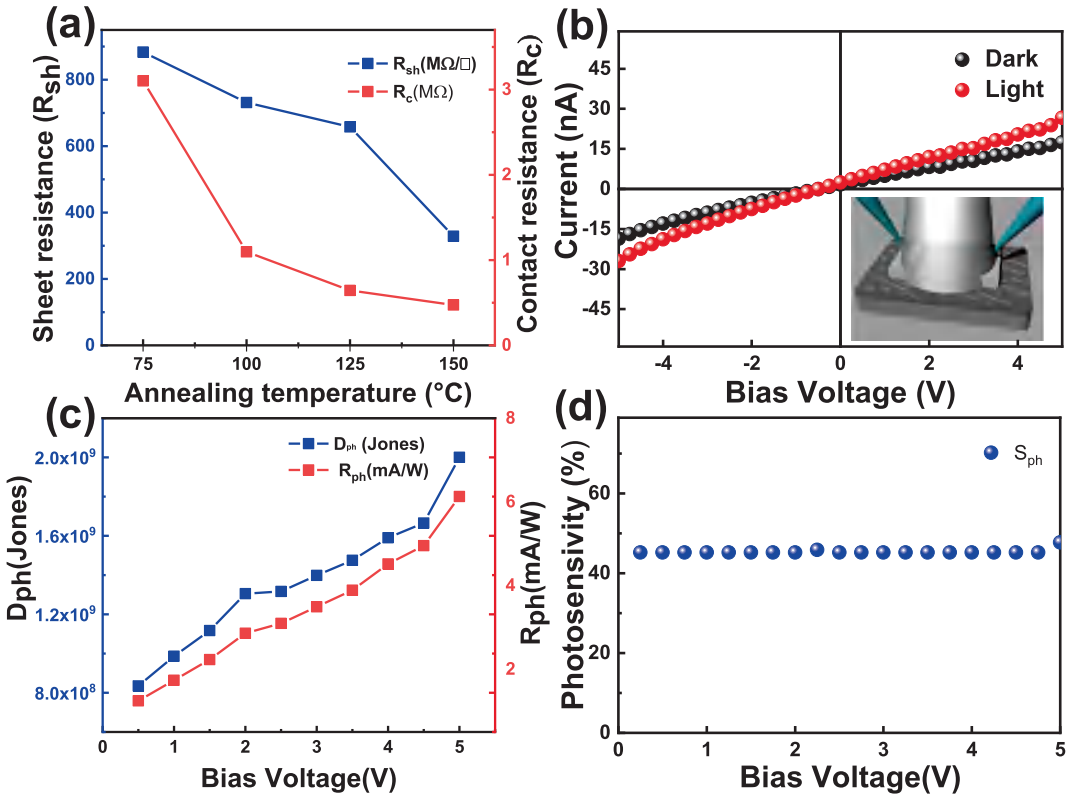

Fig. 3. (a) Electrical properties of two-terminal devices with CSI films annealed at different temperature for 30 min in a vacuum oven, and photodetection properties of CSI films at 100 °C for 30 min: (b) I-V under illumination of halogen lamp (2.5 mW/cm^2), (c) R_{ph}, D_{ph} and (d) S_{ph} values with bias voltages.

Sn, and I, are confirmed by survey spectra (Fig. S13a). The fitted core levels spectra of Cs, Sn, and I are shown in Figs. 2e–h and S14. The fitted core-level spectra of Cs3d can be assigned to two peaks, respectively, according to Cs3d$_{5/2}$, Cs3d$_{3/2}$ (Fig. S7a). The binding energy position of Cs3d$_{5/2}$ is found to be 724.2 eV, 725.3 eV for CSI films processed with 1.60 mmol, 2.00 mmol CsI, respectively (Fig. 2f). The location of binding energy at 725.3 eV confirmed the existence of the CsI along with CSI films prepared with 2mmolCsI [2]. The difference between these two peaks is estimated to be 14.68 eV, which confirms the Cs^{1+} valence state in fabricated films [2]. Apart from these peaks, additional peaks at 727.27 eV, 741.66 eV are noticed in CSI films fabricated with 2 mmol CsI concentration and which can be attributed to Cs-Cs binds [16]. The Sn 3d$_{5/2}$ and Sn 3d$_{3/2}$ regions are deconvoluted into two peaks at 486.95 eV- 487.51 eV, 484.5 eV, 495.95 eV- 496.26 eV, 494.44 eV respectively. The presence of peaks at 484.5 eV and 494.44 eV peak confirm the existence of Sn^{+4}/Sn^{+2} valence states in both fabricated films (Fig. S14) [16,17]. The difference between the doublets of Sn3d (Sn3d$_{5/2}$, Sn3d$_{3/2}$) is estimated to be 8.4 eV. The I3d doublets of CSI films fabricated with 2 mmol CsI are deconvoluted into I3d$_{5/2}$ (620.70 eV) and I3d$_{3/2}$ (632.21 eV) and which is ascribed to the triiodide I_3^- valence state [18]. Apart from these, impurity/satellite peaks at 623.3 eV and 634.89 eV are noticed, and these might correspond to the I_2O_5 phase [17]. Similarly, The I3d doublets of CSI films fabricated with 1.6 mmol CsI show two peaks and these peaks are deconvoluted into I3d$_{5/2}$ (618.98 eV, 620.70 eV) and I3d3$_{/2}$ (629.98 eV, 631.69 eV). In addition, these are associated with I^- (618.98 eV and 629.98 eV) and triiodide I_3^- (620.70 eV and 631.69 eV) valence states. Finally, XPS analysis identifies that Cs^{1+}/Cs^{2+}, Sn^{2+}/Sn^{4+}, I_3^- and Cs^{1+}, Sn^{2+}/Sn^{4+} and I^-/I_3^- valence state exist in CSI films fabricated with 2 mmol and 1.6 mmol CsI concentrations, respectively.

The detailed calculations of electrical and photodetector properties are given in the Supporting information (Fig. S15–S20). Both contact resistance (R_c) and sheet resistance (R_{sh}) decrease with an increase in the annealing temperature (Fig. 3a). The highest R_{sh} (or R_c) is found to be 880.48MΩ/sq. (or 3.10 MΩ) for 75 °C and the lowest 328.83MΩ/sq. (or 0.47 MΩ) is obtained for films annealed at 150 °C. The high R_{sh} and R_c might be due to the low density of sub-μm-sized rods, inadequate coverage of submicron-rods, change in elemental composition, and iodine deficiency [6–10]. I-V characteristics of fabricated CSI devices, CSI films annealed at 100 °C, under the illumination of halogen lamp (2.5 mW/cm^2), and dark conditions are shown in Fig. 3(b). The increase in photoresponsivity (R_{ph})/specific detectivity (D_{ph}) values are noticed while an increase in bias voltage (Fig. 3c). The highest S_{ph} and R_{ph} (or D_{ph}) is calculated to be 45% (Fig. 3d) and 6 mA/W (or 2.00 × 10^{9}Jones), at 1 V bias voltage, respectively. The performance of CSI devices can be improved by morphology optimization and reduction of iodine deficiency. The preliminary results on photodetection properties suggested that it can be utilized as a visible photodetector.

4. Conclusions

Earth-abundant, air-stable, lead-free Cs_2SnI_6 perovskite thin films have been successfully prepared on thermally oxidized Si substrate via spin coating technique at low temperature (75 ℃ for 15 min) in ambient conditions (RH < 40%). The CsI concentration and annealing temperature are clearly identified to affect the chemical composition, morphology, and phase purity of CSI films. The low-temperature processing of CSI films and the

preliminary results on photo detection properties could be potentially informative for future flexible photodetector.

CRediT authorship contribution statement

Mokurala Krishnaiah: Visualization, Writing - original draft, Validation, Investigation, Methodology, Conceptualization. **Md. Mohibul Islam Khan:** Writing - review & editing, Methodology. **Ajith Kumar:** Writing - review & editing, Methodology. **Sung Hun Jin:** Writing - review & editing, Supervision, Funding acquisition, Project administration, Resources.

Declaration of Competing Interest

The authors declare that they have no known competing financial interests or personal relationships that could have appeared to influence the work reported in this paper.

Acknowledgment

This work was supported by the Post-Doctor Research Program (2015) through Incheon National University (INU), Incheon, and the Republic of Korea.

Appendix A. Supplementary data

Supplementary data to this article can be found online at https://doi.org/10.1016/j.matlet.2020.127675.

References

[1] B. Lee, C.C. Stoumpos, N. Zhou, et al., J. Am. Chem. Soc. 136 (2014) 15379–15385.
[2] J.C.R. Ke, D.J. Lewis, A.S. Walton, et al., J. Mater. Chem. A 6 (2018) 11205–11214.
[3] A. Wang, X. Yan, S. Sun, et al., Chem. Mater. 28 (2016) 8132–8140.
[4] S. Ghosh, S. Paul, S.K. De, Part. Part. Syst. Charact. 35 (2018) 1800199–1800206.
[5] H. Shin, B.M. Kim, et al., Adv. Energy Mater. Adv. Energy Mater. 9 (2019), 1803243(8).
[6] B. Saparov, J.P. Sun, W. Meng, Z. Xiao, et al., Chem. Mater. 28 (2016) 2315–2322.
[7] T.C. Dang, H.C. Le, D.L. Pham, et al., J. Alloys Compd. 805 (2019) 847–851.
[8] B. Lee, A. Krenselewski, S. Baik, et al., Sustain, Energy Fuels 1 (2017) 710–724.
[9] F. Guo, Z. Lu, D. Mohanty, T. Wang, et al., Mater. Res. Lett. 5 (2017) 540–546.
[10] B. Lee, B. Shin, B. Park, Electron. Mater. Lett. 15 (2019) 192–200.
[11] Y. Jiang, H. Zhang, X. Qiu, B. Cao, Mater. Lett. 199 (2017) 50–52.
[12] W. Zhu, G. Xin, X. Min, et al., J. Mater. Chem. A 6 (2018) 2577–2584.
[13] W. Zhu, T. Yao, J. Shen, W. Xu, et al., J. Phys. Chem. C 123 (2019) 9575–9581.
[14] X. Wu, J. Wang, E.K.L. Yeow, J. Phys. Chem. C 120 (2016) 12273–12283.
[15] E. Horváth, M. Spina, Z. Szekrényes, et al., Nano Lett. 14 (2014) 6761–6766.
[16] L. Dimesso, C. Das, T. Mayer, Mater. Chem. Phys. 197 (2017) 27–35.
[17] A.V. Naumkin, A. Kraut-Vass, S.W. Gaarenstroom, C.J. Powell, NIST Standard Reference Database 20, version 4.1, http://srdata.nist.gov/xps/.
[18] G.R. Kumar, H.J. Kim, S. Karupannan, et al., J. Phys. Chem. C 121 (2017) 16447–16453.